5th International Conference on Experimental Fluid Mechanics – ICEFM 2018 Munich
Munich, Germany, July 2-4, 2018

Turbulent boundary layer over a wall roughened by pyramidal elements

Gaetano M Di Cicca[1*] and Michele Onorato[2]

[1] Politecnico di Torino, Dipartimento di Ingegneria Meccanica e Aerospaziale, Turin, Italy

[2] Accademia delle Scienze di Torino, Turin, Italy

*gaetano.dicicca@polito.it

Abstract

The turbulent boundary layer over a wall roughened by pyramidal elements was the subject of experimental studies at the Aeronautical Laboratory of the Politecnico di Torino. Previous studies on the subject are reported in Di Cicca et al. (2014), Di Cicca and Onorato (2016) and Di Cicca et al. (2018). PIV measurements at relatively low Reynolds numbers were carried out in a closed-loop water tunnel. The ratio between the boundary layer thickness and the pyramidal roughness height is δ/k=17.2 . The results point out the influence of the roughness on the flow in terms of mean and fluctuating quantities and turbulence scales.

1 Introduction

The geometry of pyramidal roughness is of particular interest (also with reference to numerical simulation) because it can be simply described in terms of the pyramid height, orientation with respect to the flow direction, face slope and roughness density. Moreover, the pyramidal geometry has a relevance to many engineering and environmental applications. The turbulent flow over walls roughened by pyramidal elements was the subject of investigations by the authors of the present paper (Di Cicca et al., 2014; Di Cicca and Onorato, 2016; Di Cicca et al., 2018) and also by other authors (see e.g. Schultz and Flack, 2009; Talapatra and Katz, 2012; Seddighi et al., 2015).
Many studies on the effect of wall roughness on turbulent boundary layer flows have been conducted and published up to now which refer to a wide variety of surface geometries, both two-dimensional and three-dimensional. The comprehensive review of Jimenez (2004) covers most of the work published on the subject till 2004. More recent references may be found (among others) in the introduction section of Hong et al. (2011), Di Cicca et al. (2014), Yuan and Piomelli (2014) and Flack et al. (2016).

2 Experimental set-up

PIV measurements have been carried out in a closed-loop open surface channel with a 350 mm wide, 500 mm high test section (Fig. 1a). Measurements were taken on a flat plate with a length of 2050 mm, in a region about 1750 mm downstream the leading edge for the canonical boundary layer case, and about 500 mm downstream the leading edge for the boundary layer developing over the three-dimensional rough wall. The pressure gradient was null along the test section. At the flat plate leading edge, the laminar-turbulent transition was imposed by sandpaper. The roughness consisted of pyramids with the diagonal of the square base oriented in the direction of the mean flow. Measurements have been taken in a streamwise wall normal plane intercepting the apex of a row of pyramids and the diagonal of the square base. In Fig. 1b the roughness geometry is shown. The pyramid slope is 28° and the gap between the pyramid bases is 1.4mm. The Reynolds number was Re_θ=1234 (Reynolds number based on the boundary layer momentum thickness, θ, and on the external velocity U_e). The ratio between the boundary layer thickness and the

pyramidal roughness height was δ/k=17.2 . The streamwise, wall normal and spanwise directions are respectively indicated by x, y and z.

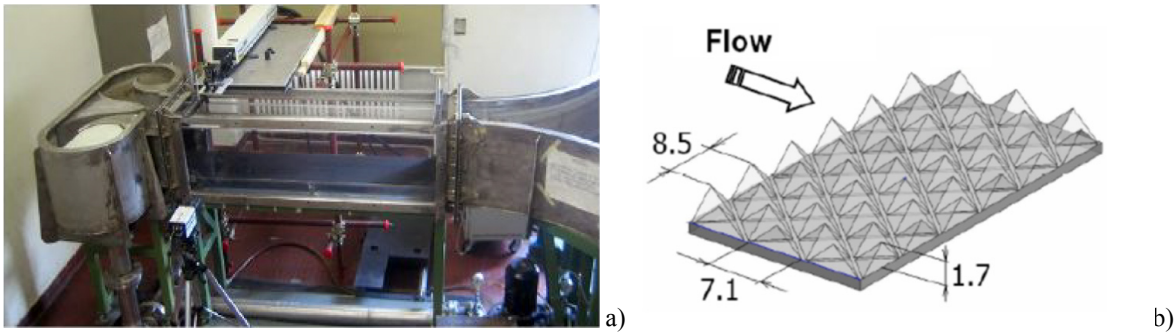

a) b)

Figure 1: a) Water tunnel; b) Roughness geometry. Dimensions in millimeters.

Measurements were taken with a particle image velocimetry system, which consisted of a 1280×1024 pixels high-speed Dantec NanoSense MKIII CMOS camera and a continuous Spectra-Physics Argon–Ion laser, with a maximum emitted power of 6W. The laser beam was expanded by a cylindrical lens and focused by a spherical lens, forming a light sheet with a thickness of about 0.5mm. The water was seeded with spherical silicon carbide particles, 2 μm nominal diameter. The physical size of the PIV images was 49.4×39.5 mm^2 (1047×840 viscous units) for the smooth wall and 42×36 mm^2 (970×831 viscous units) for the rough wall. In both cases, the PIV images covered the whole boundary layer thickness. The PIV image analysis was done using the 'LaVision DAVIS 7.2' software. The final interrogation window size was 32×32 pixels, overlap of 50%. Each velocity vector is representative of the mean velocity in an area of 1.24×1.24 mm^2 (26×26 wall units) for smooth wall and 1.06×1.06mm^2 (24×24 wall units) for rough wall. The camera acquisition rate was 800 frames per second, but for the statistical analysis only one image pair each 100 frames was recorded. Therefore, the effective acquisition rate of PIV image pairs was 8 Hz. Thirty-three hundred statistically independent image pairs were recorded to ensure the convergence of the computed averaged quantities.
The flow conditions are reported in Table 1.

Table 1: Experimental flow conditions.

Wall Surface	U_e	δ	θ	Re_θ	U_τ	U_τ/U_e	δ/k
	[m/s]	[mm]	[mm]		[m/s]		
Smooth Wall	0.485	27.95	2.99	1471	0.0213	0.044	
Rough Wall	0.36	29.29	3.79	1234	0.0255	0.071	17.2

The error in measuring the instantaneous velocity was estimated to be less than 1%. The error becomes 1.41 times higher when calculating the variance of the velocities, whereas it is negligibly small when calculating mean values. The uncertainty in the evaluation of the friction velocity U_τ , according to the modified Clauser chart method proposed by Perry and Li (1990), is equal to 3% for the smooth wall and 5% for the rough wall.

3 Results

In Fig. 2 the streamwise component of the mean velocity $\widetilde{U}^+$ and the Reynolds shear stresses $-<\widetilde{u'v'}>^+$ are visualized in a region covering a wavelength λ_x from the top of one generic pyramid to the top of the next one. y_T is the wall normal distance from the pyramid apex. The symbol tilde denotes quantities

obtained spatially averaging values in corresponding points of each region covering a wavelength λ_x and the superscript plus indicates quantities in wall units. In the figure, the wall roughness is sketched. The white triangles represent the pyramids highlighted by the laser sheet. The dark triangle represents the row of pyramids standing between the laser sheet and the observation video camera. The flow appears to be homogeneous in the streamwise x-direction for $y_T > k$ ($y/\delta > 0.08$). In the pyramid region the flow is dominated by the geometry of the roughness. Even if the flow field is not completely observable because in part shaded by the row of the dark pyramids sketched in the figures, regions of low values of $\widetilde{U}^+$ are evident downstream the pyramid in the region closer to their base (Fig. 2a). This flow clearly contributes to the increased drag of the roughened surface with respect to the smooth one. In Fig. 2b the Reynolds shear stress shows different behaviors in the two sides of the pyramids: higher values in the downstream side, with a peak of $-<\widetilde{u'v'}>^+ \cong 1.6$ and about half of this value in the upstream side. In the region between two successive pyramids $-<\widetilde{u'v'}>^+$ also shows a relatively high value around $-<\widetilde{u'v'}>^+ \cong 1$.

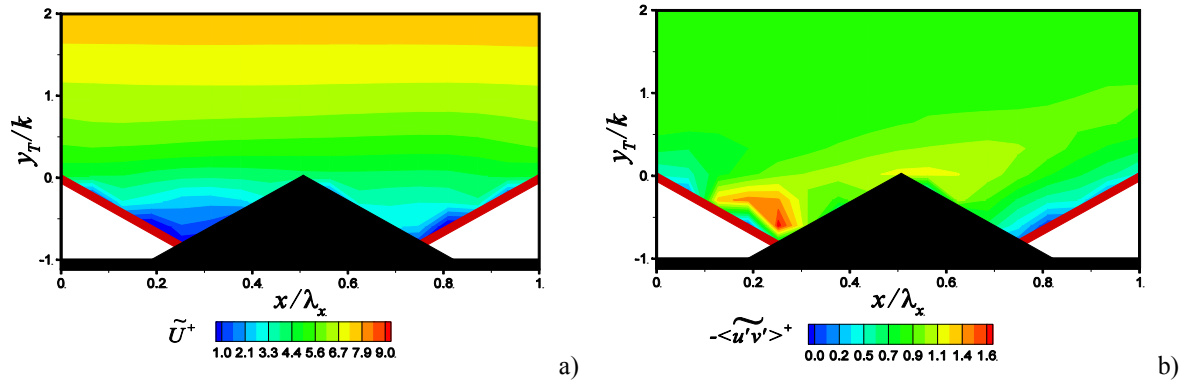

a) b)

Figure 2: a) Streamwise component of the mean velocity. b) Reynolds shear stresses.

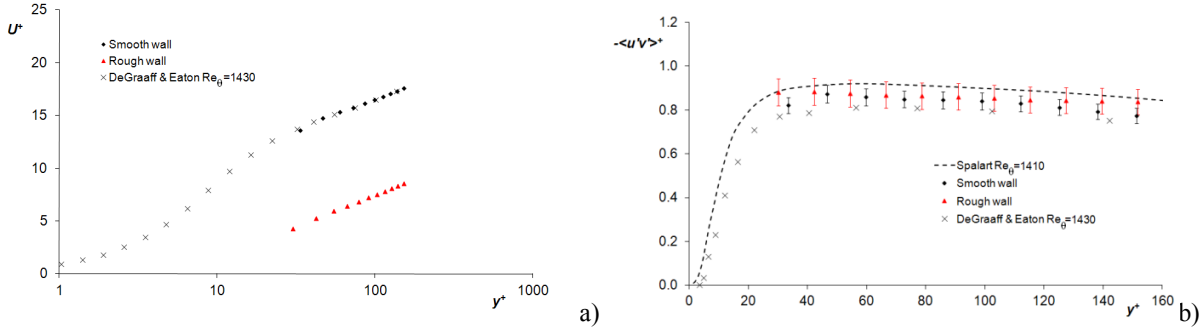

a) b)

Figure 3: a) Mean velocity profiles; b) Reynolds shear stress profiles.

In order to compare the flow behavior along the pyramidal roughened wall with the smooth wall case, quantities averaged in time and along the streamwise x-direction are shown in the following. Moreover, the concept of virtual origin has been adopted for the rough case to indicate the distance from the wall y. The virtual origin was evaluated according to Perry and Li (1990) at 1.27mm below the pyramid top. Mean velocity profiles plotted in inner variables are shown in Fig.3a for the two flows. The first measurement point reported in Fig.3a for the rough surface is located above the pyramid apex. The smooth wall Laser Doppler Velocimetry measurements of DeGraaff and Eaton (2000) at Re_θ=1430 are also reported for comparison. The rough surface displays a linear log region shifted below the smooth profile of a quantity corresponding to the roughness function, ΔU^+=8.9. The Reynolds shear stress

distributions $-<u'v'>^+$ are displayed in Fig.3b. In order to analyse the Reynolds shear stress distributions more appropriately, uncertainty bars of 4.5% and 7% are indicated for the smooth wall and the rough wall case respectively. The Spalart (1988) direct numerical simulation results for the smooth wall are reported in addition to the DeGraaff and Eaton data. The present smooth wall results are situated in between the DeGraaff and Eaton and the Spalart results. As to the comparison between the present smooth and rough wall cases, differences (of the order of 7%) are observed in proximity of the wall, where higher values of $-<u'v'>^+$ for the rough wall are detectable.

Results showing the influence of the wall roughness geometry on orientation and scales of the large turbulent structures is shown in Fig. 4, where the streamwise velocity auto-correlation function $\rho_{u'u'}$ for the rough and the smooth wall cases are compared. The extent of the regions where $\rho_{u'u'}$ is 0.6 has been chosen to be representative of the topology and the dimension of the structures. The shape of the contours $\rho_{u'u'}$ for the rough wall is qualitatively similar to the one for the case of the smooth wall. They appear elongated in the mean flow direction and inclined at a shallow angle α to the wall. The long extension of the u'-correlation is associated with the induction of the assembly of hairpin vortices in a coherent packet. The inclination angle, α, of the contours $\rho_{u'u'}$ defines the orientation of these dominant flow structures. Looking at the results in Fig. 4, for $(y/\delta)_{ref}$=0.1, $(y/\delta)_{ref}$=0.2 and $(y/\delta)_{ref}$=0.3 , an inclination angle α equal to about 11° of the contours $\rho_{u'u'}$ =0.6 is found, for both smooth and roughened surfaces (similar values of the inclination angle have been reported in Di Cicca et al. (2014) for the present data for wall distances up to $(y/\delta)_{ref}$=0.5). Very close values of α were measured in most published investigations at similar wall distances Christensen and Adrian (2001). The effect of the wall roughness on the extension of $\rho_{u'u'}$ correlation is evident very near the wall at $(y/\delta)_{ref}$=0.1, where the longitudinal length scale for the smooth surface case is larger than the one for the rough surface case. This behaviour indicates a break-up of the near-wall streamwise vortices over the rough wall. The length scale in the y-direction for the case of rough wall appears to be only slightly smaller with respect to the case of smooth wall at $(y/\delta)_{ref}$=0.1 and about comparable at $(y/\delta)_{ref}$=0.2 and $(y/\delta)_{ref}$=0.3.

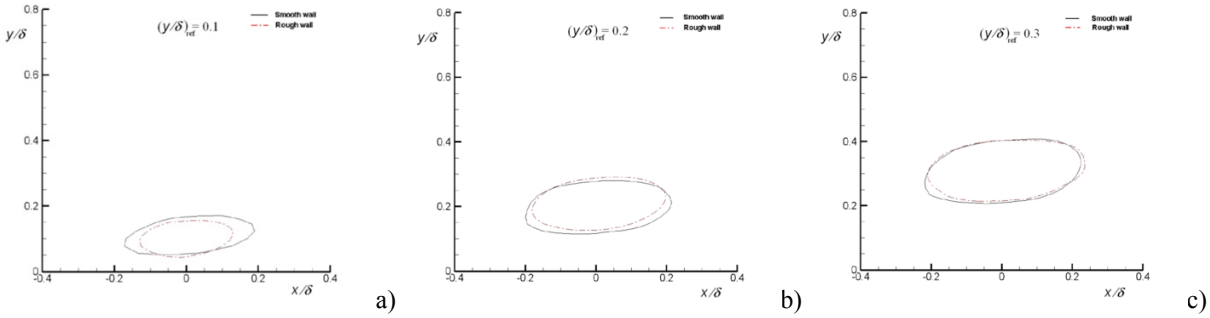

Figure 4: Contours of constant values of the two-point streamwise velocity autocorrelation function ($\rho_{u'u'}$= 0.6) for three reference distances from the wall: a) $(y/\delta)_{ref}$ = 0.1 ; b) $(y/\delta)_{ref}$ = 0.2; c) $(y/\delta)_{ref}$ = 0.3 .

The behaviour of the integral length scales in the smooth and rough wall cases can be seen in Fig. 5, where the distribution of the integral length scales, L_{11}, are reported in function of y^+.

L_{11} is defined as: $L_{11} = \int_0^\infty \rho_{u'u'}(x)dx$. At a large distance from the wall (y/δ>0.2 corresponding to y^+>150), the effect of the roughness tends to vanish, while it is very evident near the surface. In correspondence of the apex of the pyramids, the integral scales for the case of the rough wall appear to be about 30% lower. This huge reduction in integral scales, besides the previously mentioned break-up of the

near-wall streamwise vortices over the rough wall, may be attributed to the eddies generated in the thin shear layers separating from the individual roughness elements, as suggested by Castro et al. (2006).

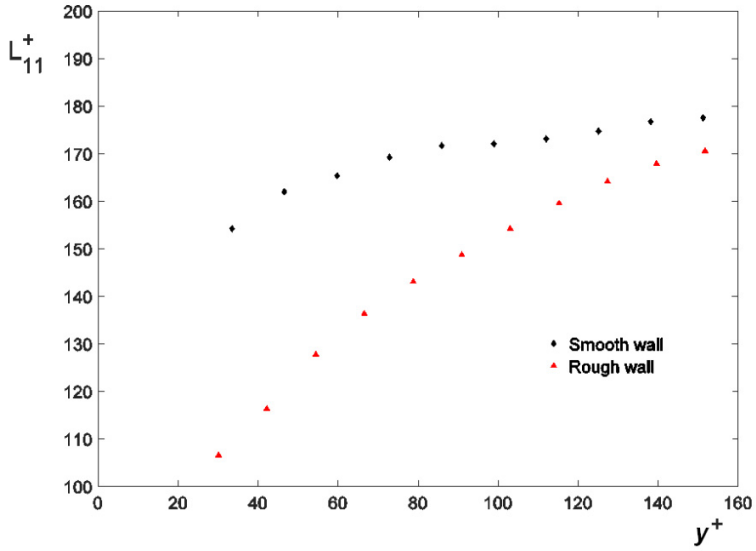

Fig.5: Integral scales L_{11}^+ in function of the distance from the wall.

4 Conclusion

All physical quantities examined for the rough wall case are shown to approach the values characterizing the smooth wall turbulent boundary layer in correspondence to the upper limit of the roughness sub-layer, evaluated at about y/δ = 0.2. Measurements very near the wall, in the roughness sub-layer, have pointed out the non-homogeneity of the flow in the streamwise direction. The different flow behaviour in the ascendant and descendent part of the pyramids and in the region between two consecutive pyramids has been visualized. Low values of the streamwise component of the mean velocity and high values of the Reynolds shear stresses are present in the region near the downstream side of the pyramids. The rough surface displays for the velocities averaged in time and along the streamwise x-direction a linear log region shifted below the smooth profile of a quantity corresponding to the roughness function, ΔU^+=8.9 . For the rough wall case, higher values of the Reynolds shear stress, averaged in time and along the streamwise x-direction, were detected in proximity of the rough surface. The two-point streamwise velocity autocorrelation function shows that the packets of hairpin vortices, populating the near wall flow, are statistically characterized by an inclination angle α equal to about 11° at $(y/\delta)_{ref}$=0.1, $(y/\delta)_{ref}$=0.2 and $(y/\delta)_{ref}$=0.3 for both smooth and roughened surfaces. Similar value (α=10° at $(y/\delta)_{ref}$=0.2) is reported by Castro et al. (2006) modeling a wall roughened by a staggered cube array. The effect of the wall roughness on the packet of hairpin structures is evident observing the extension of $\rho_{u'u'}$ contours near the wall. They show that the longitudinal length scale of the large structures for the smooth surface case is larger than the one for the rough surface case. Namely, at the distance from the wall nearly corresponding to the pyramid apex, the integral scales for the case of the rough wall appear to be about 30% smaller. This huge reduction is attributed to the break-up of the near-wall streamwise vortices over the rough wall and to the contribution of flow structures generated in the thin shear layers separating from the individual roughness elements.

References

Castro IP, Cheng H, Reynolds R (2006) Turbulence over urban-type roughness: deductions from wind tunnel measurements. *Boundary-Layer Meteorol.* 118: 109–131

Christensen KT, Adrian RJ (2001) Statistical evidence of hairpin vortex packets in wall turbulence. *J. Fluid Mech.*, 431: 433-443

DeGraaff DB, Eaton JK (2000) Reynolds-number scaling of the flat-plate turbulent boundary layer. *J. Fluid Mech.* 422: 319-346

Di Cicca GM, Ferrari A, Onorato M (2014) PIV investigation of a turbulent boundary layer over a three-dimensional rough wall. *Memorie della Accademia delle Scienze di Torino. Classe di Scienze Fisiche Matematiche e Naturali* 38:45-86

Di Cicca GM, Morvan P, Onorato M (2018) Turbulence investigation in the roughness sub-layer of a near wall flow. *Environ. Fluid Mech.* In Press.

Di Cicca GM, Onorato M (2016) Roughness sub-layer investigation of a turbulent boundary layer. *J. of Turbulence* 17(1):51-74

Flack KA, Schultz MP, Barros JM, Kim YC (2016) Skin-friction behavior in the transitionally-rough regime. *Int. J. Heat Fluid Flow* 61: 21–30

Hong J, Katz J, Schultz P (2011) Near-wall turbulence statistics and flow structures over three-dimensional roughness in a turbulent channel flow. *J. Fluid Mech.* 667: 1-37

Jiménez J (2004) Turbulent flows over rough walls. *Annu. Rev. Fluid Mech.* 36: 173-196

Perry AE, Li JD (1990) Experimental support for the attached-eddy hypothesis in zero-pressure gradient turbulent boundary layers. *J. Fluid Mech.* 218: 405-438

Schultz MP, Flack KA (2009) Turbulent boundary layers on a systematically varied rough wall. *Phys. Fluids* 21:015104

Seddighi M, He S, Pokrajac D, O'Donoghue T, Vardy AE (2015) Turbulence in a transient channel flow with a wall of pyramid roughness. *J. Fluid Mech.* 781:226-260

Spalart PR (1988) Direct simulation of a turbulent boundary layer up to $Re_\theta = 1410$. *J. Fluid Mech.* 187: 61-98

Talapatra S, Katz J (2012) Coherent structures in the inner part of a rough-wall channel flow resolved using holographic PIV. *J. Fluid Mech.* 711:161-170

Yuan J, Piomelli U (2014) Estimation and prediction of the roughness function on realistic surfaces. *J. of Turbulence*, 15(6): 350-365